Physical Science International Journal

25(6): 48-63, 2021; Article no.PSIJ.74836
ISSN: 2348-0130

Analysis of Beam Bending with an Elliptical Cross-Section

Sydney Roth[1], Mohamed Abuhegazy[1,2] and Tariq Khraishi[1*]

[1]Mechanical Engineering Department, University of New Mexico, Albuquerque, New Mexico, USA.
[2]Mechanical Power Engineering Department, Faculty of Engineering, Shebin El-Kom, Menoufia University, Egypt.

Authors' contributions

This work was carried out in contribution among all authors. Author MA was responsible for the derivations, calculations, and resulting figures. Author SR was responsible for the write-up and analysis explanation for this research. Author TK reviewed this paper and served as an advisor during the research for this paper. All authors read and approved the final manuscript.

Article Information

DOI: 10.9734/PSIJ/2021/v25i630265
Editor(s):
(1) Prof. Shi-Hai Dong, National Polytechnic Institute, Mexico.
(2) Dr. Roberto Oscar Aquilano, University of Rosario (UNR), Argentina.
Reviewers:
(1) N. Yathisha, ATME College of Engineering, India.
(2) Abel Idrisu Shaba, Federeal University of Technology Minna, Nigeria.
Complete Peer review History: https://www.sdiarticle4.com/review-history/74836

Original Research Article

Received 06 August 2021
Accepted 12 October 2021
Published 22 October 2021

ABSTRACT

This paper calculates the stress function constants to determine and analyse the stress field of a beam with an elliptical cross-section under transverse loading. This was performed using linear elasticity principles. The Beltrami-Michell compatibility equations were used to derive the formulas used to calculate these parameters in the beam with the elliptical cross-section. This paper uses dimensionless analysis to comprehend the effect of each variable in the problem. The loading was applied at the centre of the right-end face of the elliptical beam. This loading configuration is the same as an existing linear elasticity problem; however, that problem models a cylindrical beam instead of an elliptical one. Thus, the existing parameters from the cylindrical model were used to verify the formulas, calculated in this paper, for the elliptical beam.

Keywords: Beam bending; elliptical cross-section; stress function.

**Corresponding author: E-mail: khraishi@unm.edu;*

1. INTRODUCTION

The elliptical cross-section of the beam in this paper is in a state of bending. Bending is the "most common form of loading" in real world applications [1]. To analyse bending mathematically, it is useful to employ linear elasticity principles.

There are various ways a beam can be loaded to undergo bending. Calculations were made for a beam bending under a transverse load. With this type of load, there is no bending due to an applied moment. This loading does, however, produce a bending moment within the beam. Transverse loading is a load applied normal to the neutral axis.

The basis for the mathematical analysis of this bending problem are the Beltrami-Michell compatibility equations. These equations are especially useful since they avoid the deformation solutions u_i (displacement field) and e_{ij} (strain field) if there are defined traction boundary conditions. These equations, therefore, allow for a streamlined process without unnecessary variables.

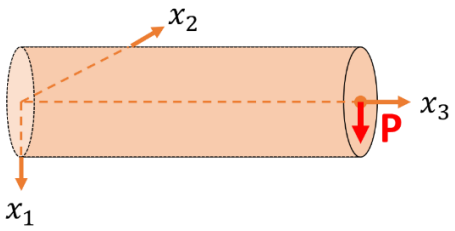

Fig. 1. Model of transverse loading of beam

Fig. 1 shows the model discussed in this paper under the transverse loading. This load is denoted by the letter P. It acts along the centre of the right end face of the beam.

These equations and relationships form the basis for the analysis of the elliptical beam presented in this paper. They provide the foundation for defining the stress function, $F = Ax_2{}^3 + Bx_1{}^2x_2 + Cx_2$, which in turn, yields the formulas for the constants A, B, and C. Since the formulas used to determine the beam stresses stemmed from the Beltrami-Michell equations, the displacement fields and the strains can be ignored in this analysis.

The setup of this problem is heavily based on the cylindrical example presented in [1].That problem uses the same methodology of determining the constants from the stress function to achieve formulas for the various stresses in the beam. Additionally, the cylindrical example is loaded identically to the problem presented in this paper.

[2] also uses a similar setup with constants to determine the formulas for the stresses in a beam with an elliptical cross-section; however, in [2], the model is a beam with half an ellipse as its cross section. The formulas in [2] use elliptical coordinates instead of using the cartesian coordinates presented in this paper to determine the equations of stress. [2] mainly analyses the aspect ratio's effect on the stresses within the elliptical cross section.

The findings of this research could be useful in analysing cylindrical beams that undergo deformation. An example of this could be beams used in the construction process. It is common for cylindrical beams to obtain elliptical cross-sections through bending [3]. [4] presents the case for a hollow beam with an elliptical cross-section under uniform loading, which transverse loading could create. This article mainly looks at how the length of a cylindrical beam affects its point of transition from having circular cross sections to an elliptical cross section.

[4] presents the same physical model as this paper, a solid homogenous beam with elliptical cross-sections. In [4] the model is in torsion, which encompasses very different calculations than for a beam under transverse loading.

The elastic properties of cylindrical beams under transverse loading have been examined in various other research work for different applications. One example of this is studying beam theory in nanoscale and microscale applications [5]. The principles of beam theory become more challenging under these smaller scales.

It is important to note that beams with other various cross-sections have been studied under the same loading as presented in this paper. For example, examining sandwich beams' stress response under transverse loading has proved to be useful for construction applications [6]. This is in addition to the study of "non-prismatic" beams, a beam that has a variable cross-section, under the loading discussed in the paper [7], [8], [9], [10]). This has applications for things such as performing stress analysis on the blades of a wind turbine [7]. References [8] and [10] focus

more on beams with variable rectangular cross-sections. Reference [10] also analyses beams with variable cross-sections.

The number of sources discussed in this paper were limited because the setup discussed in this paper was unique compared to most articles about stresses in bended beams and articles about beams with elliptical cross-sections.

2. METHODOLOGY

In Fig. 2, the ellipse's minor axis contains b. The major axis has a along it. P is the load that is on the centre of the right-end face of the beam. Only the axes x_1 and x_2 are shown here. This is because this is the front view of just the elliptical cross-section. There is, in fact, an x_3 axis as well, which would represent the length of the beam.

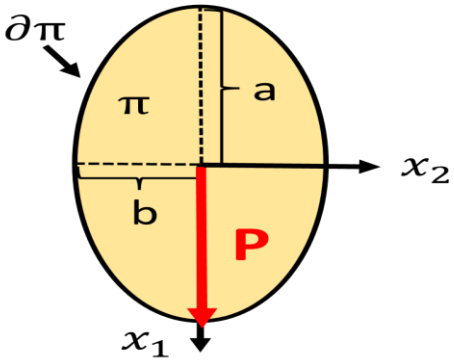

Fig. 2. Elliptical cross-section of the beam with loading

The moment of inertia for the beam is written as:

$$I = \frac{\pi}{4}ab^3 \tag{1}$$

The lateral boundary, $\partial\pi$, will be denoted by:

$$\left(\frac{x_1}{a}\right)^2 + \left(\frac{x_2}{b}\right)^2 = 1 \tag{2}$$

Assuming the stress function to be:

$$F = A{x_2}^3 + B{x_1}^2 x_2 + Cx_2 \tag{3}$$

$$\begin{cases} \nabla^2 F = \frac{v}{1+v}\frac{P}{I}\,x_2 - 2\beta\mu \\ \frac{dF}{ds} = \frac{P}{2I}\,{x_1}^2\frac{dx_2}{ds} \end{cases} \text{ on } \pi \tag{4}$$

on ∂π

Equation (8.21) for the stress function is written as [1]:

Where π represents the cross-section, ∂π is the boundary, v is Poisson's ratio, β is the twist per unit length of the beam at the centroid, and s is a curvilinear parameter measuring length around ∂π. The second of equations (4) stem from the fact that the stress traction vector is null along the surface of the beam.

Since P acts in the centre, $\beta = 0$. The equation above becomes:

$$\nabla^2 \mathrm{F} = \frac{v}{1+v}\frac{P}{I}\,x_2 \tag{5}$$

The last two equations give:

$$\nabla^2 F = \frac{\partial^2 F}{\partial {x_1}^2} + \frac{\partial^2 F}{\partial {x_2}^2} = 2Bx_2 + 6Ax_2 \tag{6}$$

This further simplifies to:

$$6A + 2B = \frac{v}{1+v}\frac{P}{I} \tag{7}$$

From the second part of equation (8.21) [1] (also the second of equations (4)):

$$\frac{dF}{ds} = \frac{P}{2I}{x_1}^2\frac{dx_2}{ds} \tag{8}$$

Additionally:

$$\frac{dF}{ds} = \frac{dF}{dx_1}\frac{dx_1}{ds} + \frac{dF}{dx_2}\frac{dx_2}{ds} \tag{9}$$

This becomes:

$$\frac{P}{2I}{x_1}^2\frac{dx_2}{ds} = 2Bx_1x_2\frac{dx_1}{ds} + (3{x_2}^2 + B{x_1}^2 + C)\frac{dx_2}{ds} \tag{10}$$

Now differentiating equation (2) with respect to s yields, after some re-arrangement:

$$\frac{dx_1}{ds} = -\frac{x_2}{x_1}\frac{a^2}{b^2}\frac{dx_2}{ds}$$

This equation is then substituted in equation (10) to have all terms involving $\frac{dx_2}{ds}$. These terms, on the left and right sides of the modified equation (10), can then be equated:

$$\frac{P}{2I}{x_1}^2 = -\frac{2a^2B}{b^2}{x_2}^2 + 3A{x_2}^2 + B{x_1}^2 + C \tag{11}$$

Re-writing equation (2):

$$x_1{}^2 = a^2 - a^2\,\frac{x_2{}^2}{b^2} \tag{12}$$

substituting the last formula back into equation (11) yields:

$$\frac{Pa^2}{2I} - \frac{Pa^2}{2Ib^2}x_2{}^2 = \left(-\frac{2a^2B}{b^2} + 3A - \frac{a^2B}{b^2}\right)x_2{}^2 + Ba^2 + C \tag{13}$$

By comparing the coefficients of the L.H.S and the R.H.S. of the equation then:

$$-\frac{Pa^2}{2Ib^2} = 3A - \frac{3a^2B}{b^2} \tag{14}$$

$$\frac{Pa^2}{2I} = Ba^2 + C \tag{15}$$

There are now three equations, equations (7), (14), and (15), that can be used to find the values for A, B, and C.

From equations (7) and (14):

$$B = \frac{P}{2I}\frac{b^2}{(3a^2 + b^2)}\left(\frac{v}{1+v} + \frac{a^2}{b^2}\right) \tag{16}$$

From equation (7);

$$A = \frac{P}{6I}\left[\frac{v}{1+v}\left(1 - \frac{b^2}{3a^2 + b^2}\right) - \frac{a^2}{3a^2 + b^2}\right] \tag{17}$$

From equation (15):

$$C = \frac{Pa^2}{2I}\left(1 - \frac{b^2}{3a^2 + b^2}\left(\frac{v}{1+v} + \frac{a^2}{b^2}\right)\right) \tag{18}$$

Solving for the stress values:

$$\sigma_{13} = F_{,2} - \frac{Px_1{}^2}{2I} = 3Ax_2{}^2 + Bx_1{}^2 + C - \frac{Px_1{}^2}{2I} \tag{19}$$

$$\sigma_{23} = -F_{,1} = -2Bx_1x_2 \tag{20}$$

$$\sigma_{33} = -\frac{P}{I}(L - x_3)x_1 \tag{21}$$

with the shear stress given by:

$$\tau = \sqrt{\sigma_{13}{}^2 + \sigma_{23}{}^2} \tag{22}$$

2.1 Comparison to Cylindrical Beam for Formula Validation

For checking these results, it is necessary to set the ellipse's major axis equal to its minor axis, $a = b$. In this case, the constant values should be the same as those for a cylindrical beam with a circular cross-section. In this section of the paper, the constants for the cylindrical constants will have the subscript labelled 'cylinder' to distinguish it from the constants for the elliptical case.

First solving for an A value in the case of $a = b$:

$$A_{cylinder} = \frac{P}{6I}\left[\frac{v}{1+v}\left(1 - \frac{a^2}{3a^2 + a^2}\right) - \frac{a^2}{3a^2 + a^2}\right] \tag{23}$$

$$A_{cylinder} = \frac{P}{6I}\left[\frac{v}{1+v}\left(\frac{3}{4}\right) - \frac{1}{4}\right] \tag{24}$$

$$A_{cylinder} = \frac{P}{24I}\left(\frac{3v}{1+v} - 1\right) = \frac{P}{24I}\left(\frac{2v-1}{1+v}\right) \tag{25}$$

Using the formulas from the ellipse problem, with $a = b$, to solve for B in the case of a circular cross-section:

$$B_{cylinder} = \frac{P}{2I}\frac{a^2}{3a^2 + a^2}\left(\frac{v}{1+v} + \frac{\cancel{a^2}}{\cancel{a^2}}\right) = \frac{P}{2I}\left(\frac{1}{4}\right)\left(\frac{v}{1+v} + 1\right) \tag{26}$$

$$B_{cylinder} = \frac{P}{8I}\,\frac{2v+1}{1+v} \tag{27}$$

Lastly, using the equations to solve for the C value:

$$C_{cylinder} = \frac{Pa^2}{2I}\left[1 - \frac{a^2}{3a^2 + a^2}\left(\frac{v}{1+v} + \frac{\cancel{a^2}}{\cancel{a^2}}\right)\right] \tag{28}$$

$$C_{cylinder} = \frac{Pa^2}{2I}\left[1 - \frac{1}{4}\left(\frac{2v+1}{1+v}\right)\right] = \frac{Pa^2}{8I}\left(4 - \frac{2v+1}{1+v}\right) \tag{29}$$

$$C_{cylinder} = \frac{Pa^2}{8I}\left(\frac{3+2v}{1+v}\right) \tag{30}$$

The results for these constants ($A_{cylinder}$, $B_{cylinder}$, and $C_{cylinder}$) are the same as the values for these constants, which describes the case of a beam with a circular cross-section undergoing transverse loading [1]. In addition, the stress field resulting from the above analysis was used to check the compatibility, equilibrium, and boundary conditions for the problem as a sanity check. It was found that the obtained stress field equations satisfied all these conditions.

2.2 Dimensionless Analysis

In this section of the paper, a superscript of a star (*) was used to denote the dimensionless variables. The following non dimensional parameters were used in the dimensionless analysis shown below:

$$x_1^* = \frac{x_1}{a}, \qquad x_2^* = \frac{x_2}{b}, \qquad x_3^* = \frac{x_3}{L}, \qquad \lambda = \frac{a}{b}$$

$$\tau^* = \frac{\tau}{P/\pi ab}, \qquad L^* = \frac{L}{b}$$

$$A^* = \frac{A}{P/\pi a^2 b^2}, \qquad B^* = \frac{B}{P/\pi a^2 b^2}, \qquad C^* = \frac{C}{P/\pi ab}$$

Using the definitions above, it is possible to solve for A^*:

$$A^* = \frac{A\pi a^2 b^2}{P} = \frac{\pi a^2 b^2}{P}\frac{P}{6\pi ab^3/4}\left[\frac{v}{1+v}\left(1-\frac{b^2}{3a^2+b^2}\right)-\frac{a^2}{3a^2+b^2}\right] \quad (31)$$

which becomes:

$$A^* = \frac{2a}{3b}\left[\frac{v}{1+v}\left(1-\frac{b^2}{3a^2+b^2}\right)-\frac{a^2}{3a^2+b^2}\right] \quad (32)$$

Using the relationship for lambda, $\lambda = \frac{a}{b}$, as defined in the previous equations:

$$A^* = \frac{2}{3}\lambda\left[\frac{v}{1+v}\left(1-\frac{1}{3\lambda^2+1}\right)-\frac{\lambda^2}{3\lambda^2+1}\right] \quad (33)$$

Next, solving for B^*:

$$B^* = \frac{B\pi a^2 b^2}{P} = \frac{\pi a^2 b^2}{P}\cdot\frac{P}{2\pi ab^3/4}\cdot\frac{b^2}{(3a^2+b^2)}\cdot\left(\frac{v}{1+v}+\frac{a^2}{b^2}\right) \quad (34)$$

$$B^* = 2\cdot\frac{a}{b}\cdot\frac{b^2}{(3a^2+b^2)}\cdot\left(\frac{v}{1+v}+\frac{a^2}{b^2}\right) \quad (35)$$

$$B^* = 2\lambda\cdot\frac{1}{(3\lambda^2+1)}\cdot\left(\frac{v}{1+v}+\lambda^2\right) \quad (36)$$

Solving for C^*:

$$C^* = \frac{C\pi ab}{P} = \frac{\pi ab}{P}\cdot\frac{Pa^2}{2\pi ab^3/4}\cdot\left[1-\frac{b^2}{(3a^2+b^2)}\cdot\left(\frac{v}{1+v}+\frac{a^2}{b^2}\right)\right] \quad (37)$$

$$C^* = 2\cdot\frac{a^2}{b^2}\cdot\left[1-\frac{b^2}{(3a^2+b^2)}\cdot\left(\frac{v}{1+v}+\frac{a^2}{b^2}\right)\right] \quad (38)$$

$$C^* = 2\,\lambda^2\left[1-\frac{1}{(3\lambda^2+1)}\cdot\left(\frac{v}{1+v}+\lambda^2\right)\right] \quad (39)$$

The next variables to solve for in the non-dimensional analysis would be the stresses, starting with

$\sigma_{13}{}^*$:

$$\sigma_{13}{}^* = \frac{\sigma_{13}}{P/\pi ab} = \frac{\pi ab}{P}\cdot\left[3Ax_2{}^2 + Bx_1{}^2 + C - \frac{Px_1{}^2}{2I}\right] \quad (40)$$

Multiplying this by $\frac{ab}{ab}$:

$$\sigma_{13}{}^* = \frac{1}{ab}\cdot\left[3\cdot\frac{A}{P/\pi a^2 b^2}\cdot x_2{}^2 + \frac{B}{P/\pi a^2 b^2}\cdot x_1{}^2 + \frac{C}{P/\pi ab}ab - \frac{\pi a^2 b^2 x_1{}^2}{2\pi ab^3/4}\right] \quad (41)$$

Using the definitions for A^*, B^*, and C^*:

$$\sigma_{13}{}^* = \frac{3A^*}{ab}x_2{}^2 + \frac{B^*}{ab}x_1{}^2 + C^* - \frac{2}{b^2}x_1{}^2 \quad (42)$$

Using the definitions for $x_1{}^*$ and $x_2{}^*$:

$$\sigma_{13}{}^* = \frac{3A^*}{\lambda}(x_2{}^*)^2 + \lambda B^*\cdot(x_1{}^*)^2 + C^* - 2\lambda^2\cdot(x_1{}^*)^2 \quad (43)$$

$$\sigma_{13}{}^* = \frac{3A^*}{\lambda}(x_2{}^*)^2 + \lambda\cdot(x_1{}^*)^2(B^* - 2\lambda) + C^* \quad (44)$$

Using the same methodology as above to solve for $\sigma_{23}{}^*$:

$$\sigma_{23}{}^* = \frac{\sigma_{23}}{P/\pi ab} = \frac{\pi ab}{P}(-2)Bx_1x_2 \quad (45)$$

Multiplying by $\frac{ab}{ab}$:

$$\sigma_{23}{}^* = -2\cdot\frac{B}{P/\pi a^2 b^2}\cdot\frac{x_1}{a}\cdot\frac{x_2}{b} \quad (46)$$

Using the above definitions for B^*, $x_1{}^*$, and $x_2{}^*$:

$$\sigma_{23}{}^* = -2B^*\cdot x_1{}^*\cdot x_2{}^* \quad (47)$$

Solving for $\sigma_{33}{}^*$:

$$\sigma_{33}{}^* = \frac{\sigma_{33}}{P/\pi ab} = -\frac{\pi ab}{P}\cdot\frac{P}{\pi ab^3/4}\cdot(L - x_3)x_1 \quad (48)$$

$$\sigma_{33}{}^* = -\frac{4}{b^2}(L - x_3)x_1 \quad (49)$$

Multiplying this by $\frac{a}{a}$:

$$\sigma_{33}{}^{*} = -4 \cdot \frac{a}{b} \cdot \frac{L}{b}\left(1 - \frac{x_3}{L}\right) \cdot \frac{x_1}{a} \tag{50}$$

Using the definitions for $L^{*}, x_1{}^{*}$, and $x_3{}^{*}$:

$$\sigma_{33}{}^{*} = -4\lambda L^{*}(1 - x_3{}^{*})\, x_1{}^{*} \tag{51}$$

Finally, the dimensionless shear stress can be calculated as:

$$\tau^{*} = \sqrt{\sigma_{13}{}^{*2} + \sigma_{23}{}^{*2}} \tag{52}$$

3. RESULTS AND DISCUSSION

From the formulas calculated in the dimensionless analysis, the effects of the variables from the equations can be studied. The variables discussed below are $\lambda, v, x_3{}^{*}$, and L^{*}. These can otherwise be referred to as the ellipse aspect ratio (λ), the ellipse beam material (v), the beam's axial position ($x_3{}^{*}$), and the beam length (L^{*}). Figs for the stress concentrations in the elliptical cross-section of the beam are shown below. This is in addition to the plots generated for the values of $x_1{}^{*}$ or $x_2{}^{*}$ versus the stress values for each mentioned variable.

The other three parameters were kept constant while analysing the effect of each specific parameter. The baseline values for these parameters were λ = 1.0, v = 0.3, $x_3{}^{*}$ = 0.5, and L^{*}= 10.

3.1 Effect of Ellipse Aspect Ratio (λ)

In order to study the impact the ellipse aspect ratio (λ) variable has on the stress field, it was necessary to choose various values for lambda keeping the other free parameters constant. This is to witness the different effects λ values have on the stress concentration diagram of the elliptical cross-section. Three values of λ were used to analyse the model given as: λ = 0.5, λ = 1.0, and λ = 2.0. It can be seen from these figures that, as the aspect ratio increases the stress values increases too.

Below is Fig. 3, which displays the $\sigma_{13}{}^{*}$ stress concentration diagrams for λ at 0.5, 1.0, and 2.0. The aspect ratio, as observed from the Figs 3.a-3.c, impacts the orientation of the cross-section as well as the stress distributions and magnitudes. From these Figs, it appears that that the maximum $\sigma_{13}{}^{*}$ value quadruples every time λ is doubled in value. By looking back at equation (44), this should not be surprising since this stress component is proportional to the square of λ. Note in Figs 3 that the $\sigma_{13}{}^{*}$ stress value is zero at the top and bottom of each of the cross-sections. This is expected from the enforcement of the zero-stress traction condition along the wall of the prismatic beam (i.e. the wall produced from extruding $\partial\pi$ along the x_3 axial direction).

The same methods used on $\sigma_{13}{}^{*}$ were applied to the dimensionless analysis equations for $\sigma_{23}{}^{*}$ to create the Fig.s 4.a-4.c below. It is important to note that changes in the maximum stress concentration are due to the change of the orientation of the ellipse with respect to the direction of the load P. This can be seen in Fig. 4 below for the $\sigma_{23}{}^{*}$ values. Additionally, the stress magnitude appears to increase linearly with the increase in aspect ratio values. According to equation (47), $\sigma_{23}{}^{*}$ increases linearly with λ. Note that the role of the σ_{23}generation in the cross-section is to combine with σ_{13}such that the total shear stress τ is always tangential in the cross-section to the perimeter and hence the zero-stress traction condition is preserved along the prismatic bar axial wall. Such results provide verification for the results of this paper.

$\sigma_{33}{}^{*}$ at the specified λ values are depicted in the stress concentration Figs 5.a-5.c below. It is shown that variation in the ellipse aspect ratio impacts the magnitude and distribution of stress as well as the orientation of the cross-section with respect to the applied load. Note the linear change in $\sigma_{33}{}^{*}$ values with λ which is expressed mathematically in equation (51). Also, note the linear change of this stress component along the x_1 direction, from the neutral axis, which is due to the bending of the beam or bar.

Next, for Fig. 6 below, the shear stress, τ^{*}, was analysed using the dimensionless equations (equation (52)), in the same manner as the stress values above with the same values for the aspect ratios. It can be noted that the aspect ratio affects the magnitude and distribution of the shear stress along with the orientation of the cross-section with respect to the loading.

Fig. 7.c below shows $x_1{}^{*}$ values versus the stress values for $\sigma_{33}{}^{*}$. Upon inspection, it appears that as the $x_1{}^{*}$ values increase the stress values decrease linearly (see above discussion). At λ = 2.0, the magnitude of the slope is the greatest of all the other lambda values. In other words, a higher aspect ratio value yields a greater change in stress along $x_1{}^{*}$.

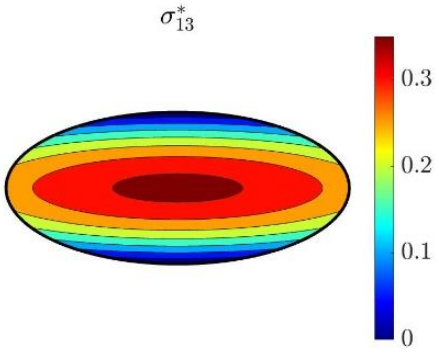

Fig. 3.a. $\sigma_{13}{}^*$ stress concentration diagram for λ = 0.5, v = 0.3, $x_3{}^*$ = 0.5, and L^* = 10

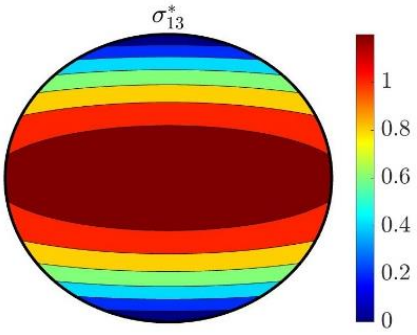

Fig. 3.b. $\sigma_{13}{}^*$ stress concentration diagram for λ = 1.0, v = 0.3, $x_3{}^*$ = 0.5, and L^* = 10

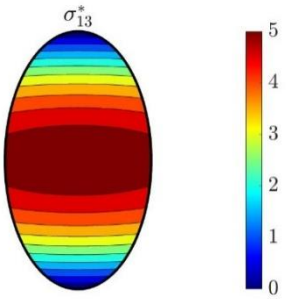

Fig. 3.c. $\sigma_{13}{}^*$ stress concentration diagram for λ = 2.0, v = 0.3, $x_3{}^*$ = 0.5, and L^* = 10

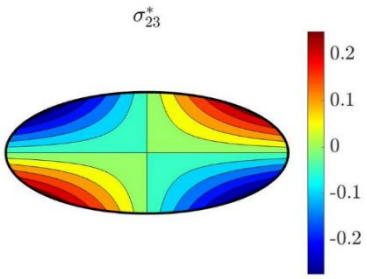

Fig. 4.a. $\sigma_{23}{}^*$ stress concentration diagram for λ = 0.5, v = 0.3, $x_3{}^*$ = 0.5, and L^* = 10

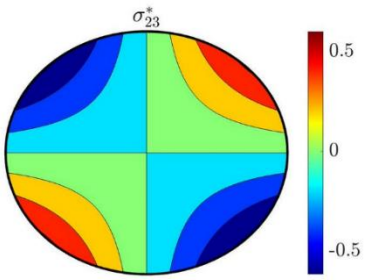

Fig. 4.b. $\sigma_{23}{}^*$ stress concentration diagram for λ = 1.0, v = 0.3, $x_3{}^*$ = 0.5, and L^* = 10

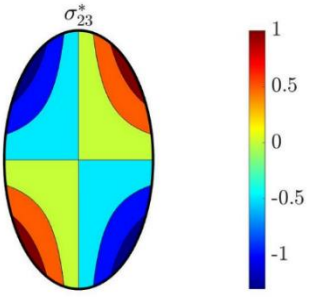

Fig. 4.c. $\sigma_{23}{}^*$ stress concentration diagram for λ = 2.0, v = 0.3, $x_3{}^*$ = 0.5, and L^* = 10

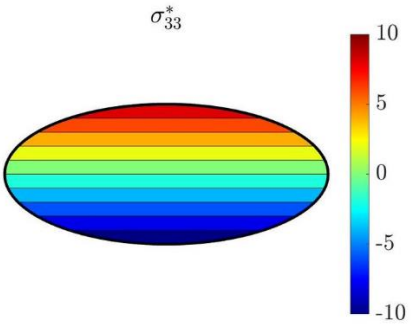

Fig. 5.a. $\sigma_{33}{}^*$ stress concentration diagram for λ = 0.5, v = 0.3, $x_3{}^*$ = 0.5, and L^* = 10

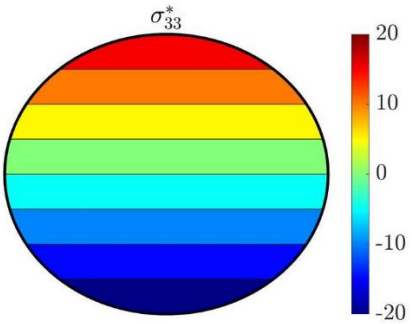

Fig. 5.b. $\sigma_{33}{}^*$ stress concentration diagram for λ = 1.0, v = 0.3, $x_3{}^*$ = 0.5, and L^* = 10

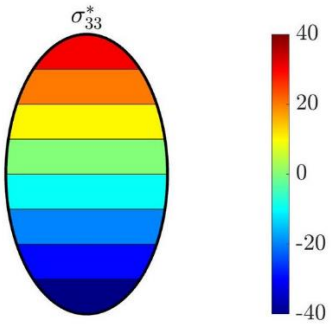

Fig. 5.c. $\sigma_{33}{}^*$ stress concentration diagram for λ = 2.0, v = 0.3, $x_3{}^*$ = 0.5, and L^* = 10

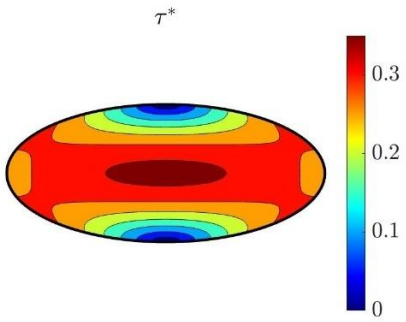

Fig. 6.a. τ^* stress concentration diagram for λ = 0.5, v = 0.3, $x_3{}^*$ = 0.5, and L^* = 10

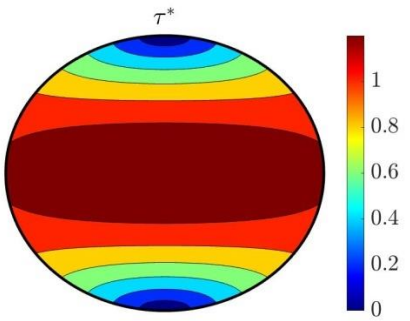

Fig. 6.b. τ^* stress concentration diagram for λ = 1.0, v = 0.3, $x_3{}^*$ = 0.5, and L^* = 10

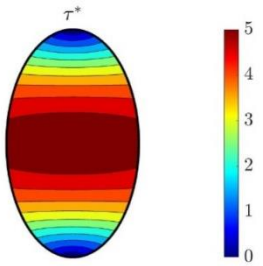

Fig. 6.c. τ^* stress concentration diagram for λ = 2.0, v = 0.3, $x_3{}^*$ = 0.5, and L^* = 10

In the plots below, τ^* was analysed along both ${x_1}^*$, Fig. 7.a, and ${x_2}^*$, Fig. 7.b. For FiZ. 7.a, λ = 2.0, again, for ${x_1}^*$, leads to the greatest change in shear stress among the other displayed lambda values (from the initial value on the plot to the final value). The relationship for the shear stress along ${x_1}^*$ is nonlinear.

For Fig. 7.b, the plot of τ^* along ${x_2}^*$, the slopes for all the lambda values seem very similar to one another. Therefore, there is no notable effect of the lambda value on the slope of τ^* along ${x_2}^*$. Also, the slopes appear to be small in value. However, it is important to note that for λ = 2.0 the shear stress is at a value greater than the other lambda parameters.

From plot 7.d. below, it can be seen that ${\tau^*}_{max}$ and ${\sigma^*}_{33_{max}}$ are proportionally related in terms of λ. As λ increases, ${\tau^*}_{max}$ and ${\sigma^*}_{33_{max}}$ also increase in value as well. ${\sigma^*}_{33_{max}}$ versus λ exhibits a linear relationship while ${\tau^*}_{max}$ with λ represent a non-linear relationship.

The ellipse aspect ratio impacting the stress values is important because it is a representation of the ratio of the major axis and the minor axis of the elliptical cross-section. This means that if an experiment was performed with the same loading set-up as presented in this paper (with an elliptical beam), the orientation of the ellipse would affect the stress values.

3.2 Effect of the Ellipse Beam Material (v)

To analyse the effect of the beam material represented by the different Poisson's ratios (ν), different values of ν were put into the stress equations from the dimensionless analysis to see how this value affects stress in the system. The parameters used were: ν = 0.1, ν = 0.3, and ν = 0.5.

Fig. 8 below shows the ${\sigma_{13}}^*$ stress concentrations for the three different values of v. It is shown that while variation in v doesn't impact the magnitude of the ${\sigma_{13}}^*$ stress, it does affect the ${\sigma_{13}}^*$ stress distribution.

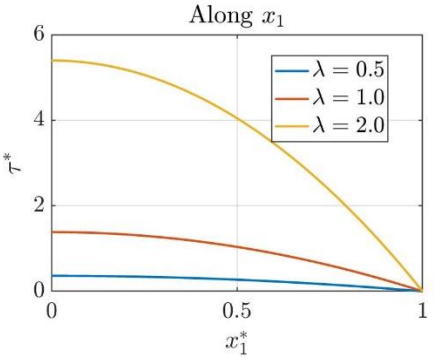

Fig. 7.a. Plot of τ^* vs. ${x_1}^*$ for λ

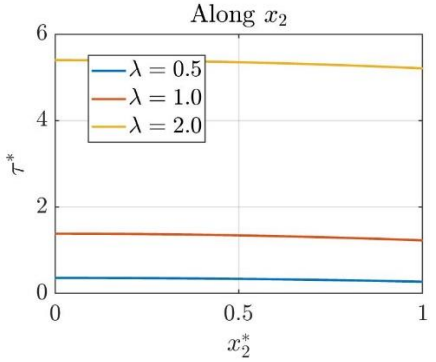

Fig. 7.b. Plot of τ^* vs. ${x_2}^*$ for λ

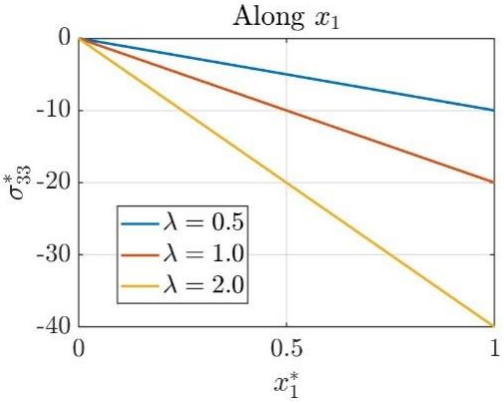

Fig. 7.c. Plot of ${\sigma_{33}}^*$ vs ${x_1}^*$ for λ

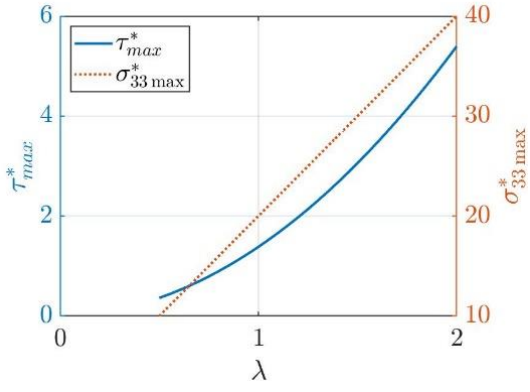

Fig.7.d. Plot of ${\tau^*}_{max}$ and ${\sigma^*}_{33_{max}}$ vs. λ

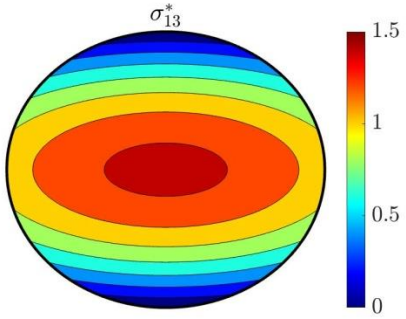

Fig. 8.a. $\sigma_{13}{}^*$ stress concentration diagram for v = 0.1, λ = 1.0, $x_3{}^*$ = 0.5, and L^* = 10

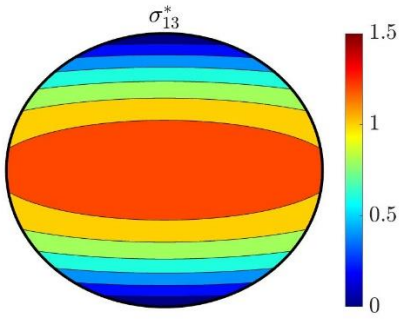

Fig. 8.b. $\sigma_{13}{}^*$ stress concentration diagram for v = 0.3, λ = 1.0, $x_3{}^*$ = 0.5, and L^* = 10

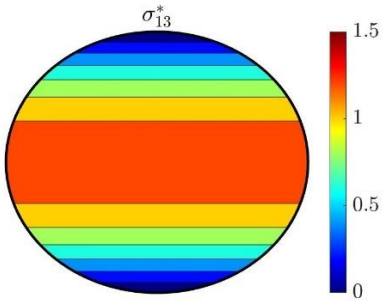

Fig. 8.c. $\sigma_{13}{}^*$ stress concentration diagram for v = 0.5, λ = 1.0, $x_3{}^*$ = 0.5, and L^* = 10

Next, the stress concentration diagrams for $\sigma_{23}{}^*$are shown in Fig. 9 below. Refer to Fig. 4.b. for the $\sigma_{23}{}^*$ stress diagram when v = 0.3. The figures below show that increasing v slightly impacts the stress values for this stress component with similar spatial distribution.

The stress concentration diagrams for $\sigma_{33}{}^*$ are identical to Fig. 5.b. for the three studied values of v, v = 0.1, v = 0.3, and v = 0.5. This suggests that v has no effect on the stress magnitude or distribution. Equation (51) shows the independence of $\sigma_{33}{}^*$ from v.

The specified values of ν were used in the dimensionless analysis equation (equation (52)) for shear stress, τ^*, to obtain Figs 10.a-10.c below. While the magnitude of the shear stress is unchanging for the different values of v, the distribution of the shear stress varies for the different Poisson's ratio values.

Fig. 11.a, shown below, demonstrates that there is an inverse relationship between increasing $x_1{}^*$ values and the shear stress, τ^*. The plot also reveals that increasing the value of v from 0.1 to 0.5 does not significantly impact the relationship between $x_1{}^*$ and τ^*. This can also be seen in Fig. 8. It is important to note that the lines describing each of the v values starts in a different place than one another with v = 0.1 starting at the highest value. This means that at v = 0.1 the cross-section centre point shear stress value is the greatest.

For Fig. 11.b, the slopes of the curves decrease after ν = 0.1 until it reaches ν = 0.5, where it is almost a straight line. Therefore, at ν = 0.1, the $x_2{}^*$ values have the greatest impact on the shear stress values. Additionally, the centre point shear stress value is the greatest at ν = 0.1. Note that there is more change in the value of τ^* with $x_1{}^*$ than with $x_2{}^*$.

Fig. 11.c reveals that the lines that describe all the various values of v are the same, thus why only the line for v = 0.5 is visible. This plot shows that $\sigma^*{}_{33}$ decreases linearly with the increase in the $x_1{}^*$ values. This independence of $\sigma^*{}_{33}$ from v is clear in equation (51).

Fig. 11.d. reveals that while the maximum shear stress value decreases as the value of Poisson's ratio increases, the axial stress $\sigma^*{}_{33_{max}}$ remains constant regardless of the value of v. Thus, v does not affect $\sigma^*{}_{33_{max}}$.

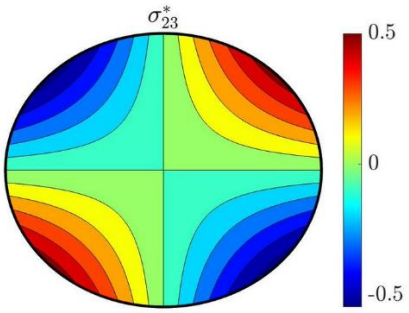

Fig. 9.a. $\sigma_{23}{}^*$ stress concentration diagram for v = 0.1, λ = 1.0, $x_3{}^*$ = 0.5, and L^* = 10

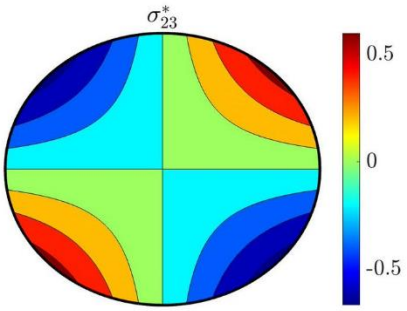

Fig. 9.b. $\sigma_{23}{}^*$ stress concentration diagram for v = 0.5, λ = 1.0, $x_3{}^*$ = 0.5, and L^* = 10

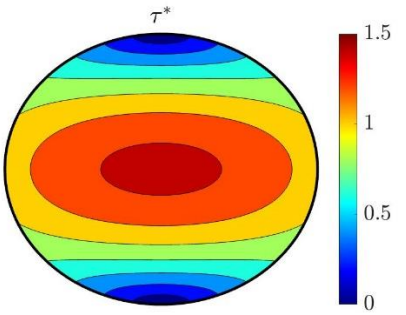

Fig. 10.a. τ^*stress concentration diagram for v = 0.1, λ = 1.0, $x_3{}^*$ = 0.5, and L^* = 10

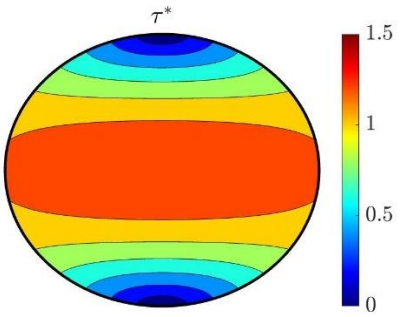

Fig. 10.b. τ^*stress concentration diagram for v = 0.3, λ = 1.0, $x_3{}^*$ = 0.5, and L^* = 10

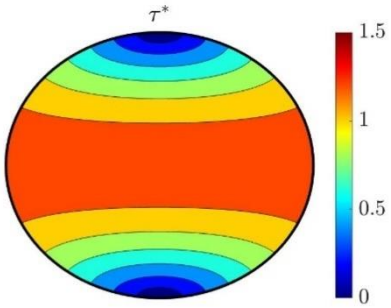

Fig. 10.c. τ^*stress concentration diagram for v = 0.5, λ = 1.0, $x_3{}^*$ = 0.5, and L^* = 10

3.3 Effect of the Beam Axial Position ($x_3{}^*$)

The impact of the beam's axial position represented by the dimensionless parameter $x_3{}^*$ on the stress values was analysed by setting $x_3{}^*$ to different values. These values were then applied in the dimensionless analysis formulas to see this parameter's effect on the stress values. The specific values used in this analysis for $x_3{}^*$ were: $x_3{}^*$ = 0.0, which is the base of the beam fixed on one side, $x_3{}^*$ = 0.5, and $x_3{}^*$ = 0.9. Since (from equations 44, 47, and 51) $x_3{}^*$ is only affecting the stress field of $\sigma_{33}{}^*$, the analysis was done for such stress field only.

Refer to Fig. 8.b. for the $\sigma_{13}{}^*$ stress concentration diagrams for when $x_3{}^*$ is 0, 0.5, and 0.9. Since the figures for these values are all identical to one another, it can be seen that change in the $x_3{}^*$ value has no impact on the $\sigma_{13}{}^*$ stress distribution or magnitude.

Refer to Fig. 4.b. for the $\sigma_{23}{}^*$ stress concentration diagrams for $x_3{}^*$ values of 0, 0.5,

and 0.9. Since the figures for all these values are the same, variation in $x_3{}^*$ has no impact on the magnitude or distribution of the $\sigma_{23}{}^*$ stress.

The Figs 12.a-12.c below show the stress concentration diagrams for $\sigma_{33}{}^*$ for different values of $x_3{}^*$. From Fig. 12 it can be noted that the distribution of $\sigma_{33}{}^*$ is uniform across x_2, and it decreases in magnitude as it moves away from the base and gets closer to the applied load. This is because of the deceasing moment value when getting close to the load. This is due to the decrease of the arm length for the moment.

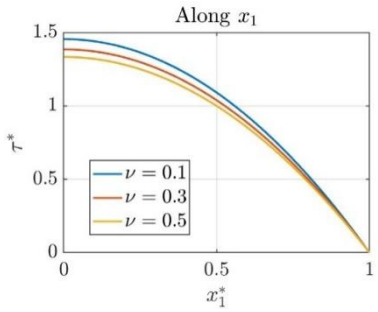

Fig. 11.a. Plot of τ^* vs. $x_1{}^*$for v

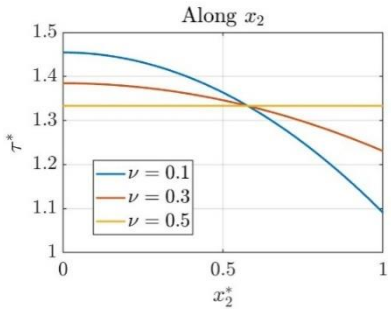

Fig. 11.b. Plot of τ^* vs. $x_2{}^*$for v

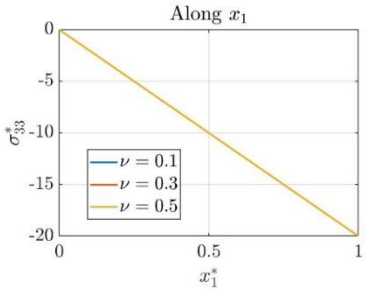

Fig. 11.c. Plot of σ_{33}^* vs. $x_1{}^*$for v

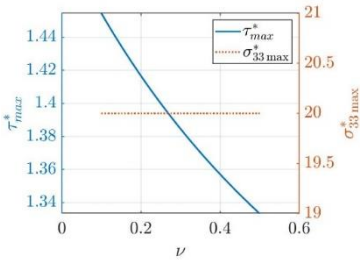

Fig. 11.d. Plot of $\tau^*{}_{max}$ and $\sigma^*{}_{33_{max}}$ vs. v

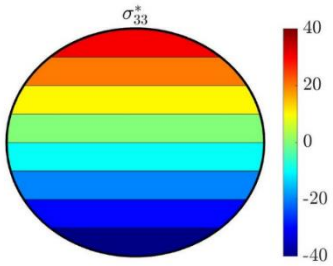

Fig. 12.a. $\sigma_{33}{}^*$ stress concentration diagram for $x_3{}^*$= 0.0, λ = 1.0, v= 0.3, and L^* = 10

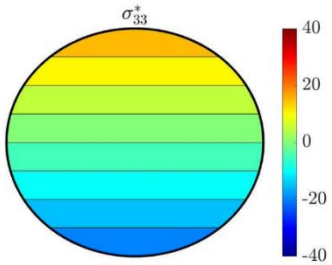

Fig. 12.b. $\sigma_{33}{}^*$ stress concentration diagram for $x_3{}^*$= 0.5, λ = 1.0, v= 0.3, and L^* = 10

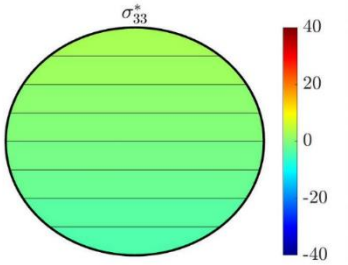

Fig. 12.c. $\sigma_{33}{}^*$ stress concentration diagram for $x_3{}^*$= 0.9, λ = 1.0, v= 0.3, and L^* = 10

Refer to Fig. 10.b for the stress diagrams for τ^* for the specified x_3^*values, 0, 0.5, and 0.9. The fact that there is not variation in the stress diagrams for the values of x_3^* shows that x_3^* does not impact the shear stress magnitude or distribution.

The figure below, Fig. 13.c, shows a plot for x_1^* versus σ_{33}^* for the specified values of x_3^*. At x_3^*= 0.0, the magnitude of the slope was the greatest compared to the other two x_3^* values. For all the specified x_3^* values, as x_1^* increases the values for σ_{33}^* decreases. Since there's a notable difference in the slopes for each of the x_3^* values, it can be concluded that the x_3^* value will impact the stress results along x_1^*.

Fig. 13.a only shows the relationship for x_3^* = 0.9, but the other lines for the various x_3^* values are under the line. In other words, the lines that describe the different values are all the same. This plot shows that the shear stress decreases with the increase in x_1^*. This relationship, however, is not linear. We have seen similar drops in Figs 11a and 7a.

Fig. 13.b is similar to 13.a. A notable difference is that 13.b has a higher shear stress value when x_2^* = 1 than 13.a, which is at 0 when x_1^* = 1. The shape of the line itself, however, has a reduced slope but similar shape. Again, x_3^* does not have an effect on τ^*.

Fig. 13.d. shows that the maximum shear stress is not impacted by changes in x_3^*. $\sigma^*{}_{33_{max}}$ is shown to be linearly related to x_3^* (see equation (51)).

3.4 Effect of the Beam Length L*

The effect of beam length, represented by the dimensionless parameter L^*, on the stress values was found by setting this variable equal to specific values and then using them in the dimensionless analysis equations. The specific values used for this parameter were: L^*= 5, L^* = 10, and L^* = 20. Again, this parameter is only affecting the stress field of σ_{33}^*. As a result, the analysis was done for such stress field only.

Fig. 8.b. is the same as the stress concentration diagrams for σ_{13}^* when L^* is 5, 10, and 20. This suggests that varying L^* values have no effect on the σ_{13}^* stress magnitude or concentration.

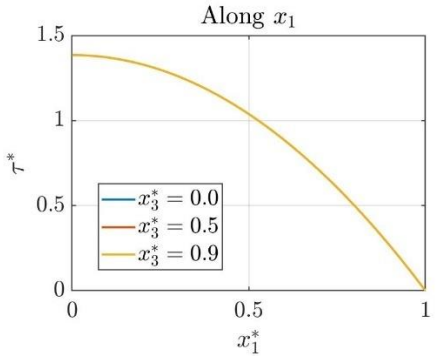

Fig. 13.a. Plot of τ^* vs. $x_1^*$for x_3^*

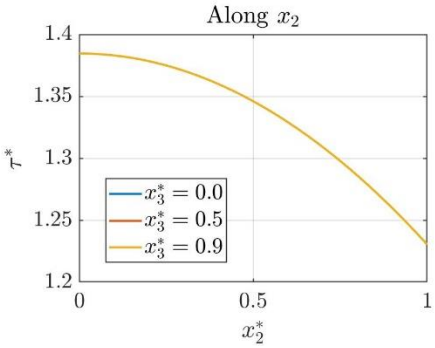

Fig. 13.b. Plot of τ^* vs. $x_2^*$for x_3^*

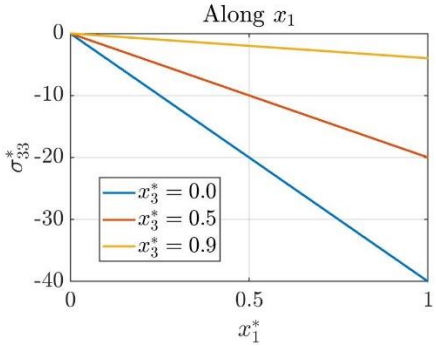

Fig. 13.c. Plot of σ_{33}^* vs. x_1^* for x_3^*

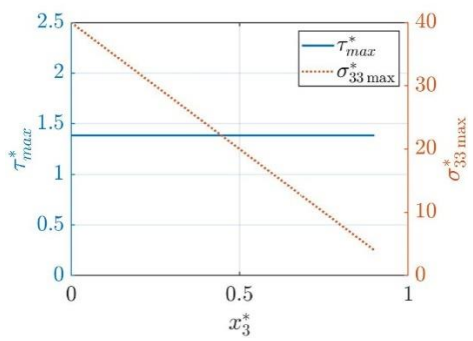

Fig. 13.d. Plot of $\tau^*{}_{max}$ and $\sigma^*{}_{33_{max}}$ vs. x_3^*

Fig. 4.b. is identical to the stress concentration diagrams for σ_{23}^* when L^* is 5, 10, and 20. This suggests that L^* has no impact on the stress magnitude or distribution since there is no change in the figures for the different values of L^*.

The stress diagram for σ_{33}^* is shown in Fig. 14 below. Fig. 5.b. is the same as the diagram for σ_{33}^* when L^* is 10. It appears that change in L^* has both an impact on the stress distribution as well as the magnitude of stress present in the cross-section.

Fig. 10.b. is representative of the stress concentration diagrams for τ^* when L^* is 5, 10, and 20. Since there is no change in the stress magnitudes and distributions between the diagrams with the different L^* values, it is seen that L^* has no effect on the τ^* stress.

Fig. 15.a shows that the same line describes the relationships for L^* at 5, 10, and 20. This is also true for Fig. 15.b, thus why both these plots only have the line for L^* = 20 visible. This additionally means that the value of L^* has no impact on the relationship between the shear stress and x_1^* or the x_2^* values.

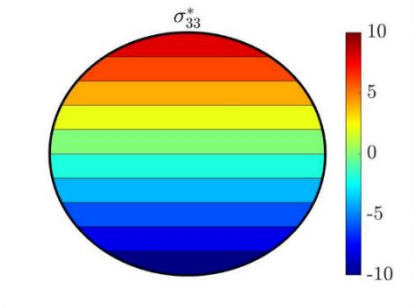

Fig. 14.a. σ_{33}^* stress concentration diagram for L^* = 5, λ = 1.0, x_3^* = 0.5, and v = 0.3

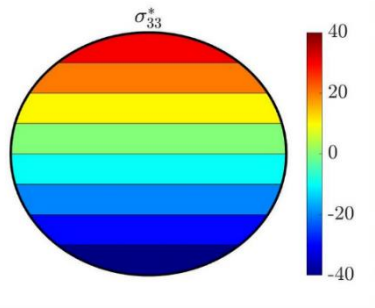

Fig. 14.b. σ_{33}^* stress concentration diagram for L^* = 20, λ = 1.0, x_3^* = 0.5, and v = 0.3

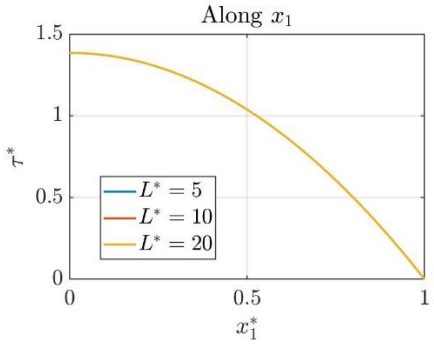

Fig. 15.a. Plot of x_1^* vs. τ^* for L^*

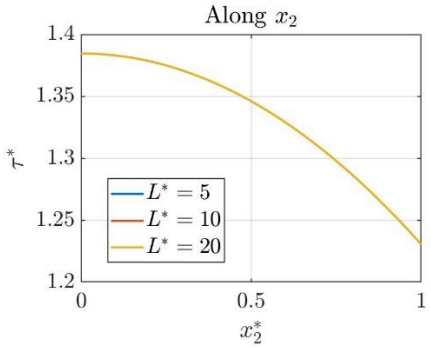

Fig. 15.b. Plot of x_2^* vs. τ^* for L^*

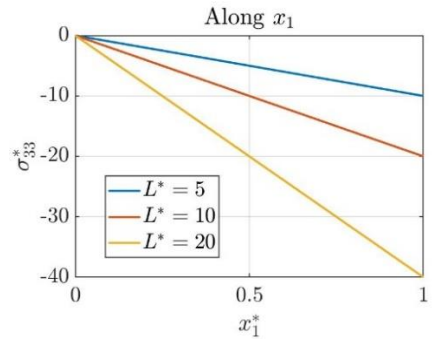

Fig. 15.c. Plot of x_1^* vs. σ_{33}^* for L^*

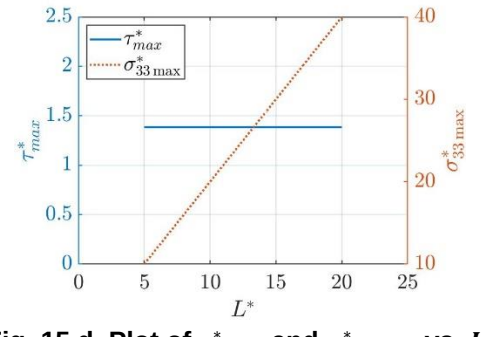

Fig. 15.d. Plot of τ^*_{max} and $\sigma^*_{33_{max}}$ vs. L^*

Fig. 15.a ends at x_1^* = 1 and τ^* = 0 while Fig. 15.b ends when x_2^* = 1 and τ^* is greater than zero. They also both have starting points that are very close in value to one another. This means that the slope for the x_1^* values is greater than the one for the x_2^* values. Both plots show an inverse relationship between the increasing shear stress values and the x_1^* and x_2^* values. It is also important to note that neither plot shows a linear relationship.

Fig. 15.c shows the relationship between $\sigma_{33}^*$and x_1^* in a plot for L^*. When L^* = 20 the magnitude of the slope is the greatest. According to the plot, as x_1^* increases σ_{33}^* decreases for any given L^*. Since the magnitudes of the slopes vary for each value of L^*, L^* affects the stress value σ_{33}^*. The plot shows this relationship as being linear between σ_{33}^* and x_1^*.

Fig. 15.d shows that the shear stress stays constant with varying $\boldsymbol{L}^*$ values, while $\boldsymbol{\sigma^*_{33_{max}}}$ is linearly proportional to the increasing $\boldsymbol{L}^*$values.

4. CONCLUSIONS

The Beltrami-Michell compatibility equations were successful in deriving a formula for analysing the stresses in a prismatic beam/bar with an elliptic cross-section, with loading along the centre of the right end on one of the cross-section axes. The resulting stress equations discovered for a beam with an elliptical cross-section differed from the equations describing the cylindrical beam. To verify, the elliptical formulas were checked in the limit for an aspect ratio of unity. This produced exactly the analytical solution for a cylindrical beam/bar presented in [1].

The variables found in the stress equations for the elliptical beam were also studied to see their effects on the stress values for the beam. This was done using dimensionless analysis. This analysis revealed that the aspect ratio had the greatest impact on the shear and normal axial stresses. The Poisson's ratio had minimal impact on the stress magnitude. Also, the beam length and axial position of a cross-section affected the axial normal stress.

The parameters studied in the Results and Discussion section for an elliptical cross-section beam had similar effects on beams with other cross-sections presented in previous research work. For example, Poisson's ratio impacted beams with other cross-sections as shown in references [2], [4], [6], [7], and [9]. The beam length was also shown to impact certain stress values in the referenced works of [2], [7], and [9].

The results from varying the ellipse aspect ratio when analysing the shear stress were very similar to the findings presented in [2]. This is because [2] notes that for larger ellipse aspect ratios the stress is located more in the "mid-plane," but as the ratio value decreases the stresses concentrates more at the "load tip." This can be seen in Fig. 6.

Through understanding the properties of ellipses and using linear elastic principles, it was possible to create new formulas that describe stresses in a beam with an elliptical cross-section under a transverse loading.

COMPETING INTERESTS

Authors have declared that no competing interests exist.

REFERENCES

1. Khraishi TA, Shen YL. Introductory Continuum Mechanics, Cognella, Inc; 2013.
2. Velazquez E, Kosmatka JB. "Stresses in a Half-Elliptic Curved Beam Subjected to Transverse Tip Forces," Journal of Applied Mechanics. 2012;80(1):2-6.
3. Xu Z, Gardner L, Sadowski AJ. "Nonlinear stability of elastic elliptical cylindrical shells under uniform bending," International Journal of Mechanical Sciences. 2017;128–129:593-606.
4. Andersen L, Nielsen SR. DCE Lecture Notes. Elastic Beams in Three Dimensions, Aalborg: Aalborg University Department of Civil Engineering. 2008;23:55-56.
5. Wang CM, Kitipornchai S, Lim CW, Eisenberger M. Beam bending solutions based on nonlocal Timoshenko beam theory," Journal of Engineering Mechanics. 2008;134:6.
6. Qin QH, Wang T. An analytical solution for the large deflections of a slender sandwich beam with a metallic foam core under transverse loading by a flat punch," Composite Structures. 2009;88(4):509-518.
7. Vilar M, Hadjiloizi D, Masjedi PK, Weaver MP. Stress analysis of generally

asymmetric non-prismatic beams subject to arbitrary loads," European Journal of Mechanics - A/Solids. 2021;9.
8. Zhou M, Fu H, An L. Distribution and Properties of Shear Stress in Elastic Beams with Variable Cross Section: Theoretical Analysis and Finite Element Modelling," KSCE Journal of Civil Engineering. 2020;24(4):1240–1254.
9. Fertis DG, Member A, Keene ME. "Elastic and inelastic analysis of nonprismatic members," Journal of Structural Engineering. 1990;116(2):475-489.
10. Baptista AM, Muzeau JP. Elastic design of tapered beam-columns subjected to concentrated axial and transversal loads," in 3rd European Conference on Steel Structures - Eurosteel Coimbra; 2002.

Peer-review history:
The peer review history for this paper can be accessed here:
https://www.sdiarticle4.com/review-history/74836